METHODS AND APPROACHES

Mechanotransduction by Membrane Proteins

A high-throughput electrophysiology assay to study the response of PIEZO1 to mechanical stimulation

Nicoletta Murciano[1,2]*, Maria Giustina Rotordam[1]*, Nadine Becker[1], Melanie J. Ludlow[4], Gregory Parsonage[4], Alexis Darras[3], Lars Kaestner[2,3], David J. Beech[4], Michael George[1], Niels Fertig[1], Markus Rapedius[1], and Andrea Brüggemann[1]

PIEZO1 channels are mechanically activated cation channels that play a pivotal role in sensing mechanical forces in various cell types. Their dysfunction has been associated with numerous pathophysiological states, including generalized lymphatic dysplasia, varicose vein disease, and hereditary xerocytosis. Given their physiological relevance, investigating PIEZO1 is crucial for the pharmaceutical industry, which requires scalable techniques to allow for drug discovery. In this regard, several studies have used high-throughput automated patch clamp (APC) combined with Yoda1, a specific gating modifier of PIEZO1 channels, to explore the function and properties of PIEZO1 in heterologous expression systems, as well as in primary cells. However, a combination of solely mechanical stimulation (M-Stim) and high-throughput APC has not yet been available for the study of PIEZO1 channels. Here, we show that optimization of pipetting parameters of the SyncroPatch 384 coupled with multihole NPC-384 chips enables M-Stim of PIEZO1 channels in high-throughput electrophysiology. We used this approach to explore differences between the response of mouse and human PIEZO1 channels to mechanical and/or chemical stimuli. Our results suggest that applying solutions on top of the cells at elevated pipetting flows is crucial for activating PIEZO1 channels by M-Stim on the SyncroPatch 384. The possibility of comparing and combining mechanical and chemical stimulation in a high-throughput patch clamp assay facilitates investigations on PIEZO1 channels and thereby provides an important experimental tool for drug development.

Introduction

The sensing of mechanical force by cells is increasingly recognized to be crucial in biology, particularly since the identities of direct, possibly dedicated, molecular mechanisms of force sensing have come to the fore. This is most obvious in the recent discovery and characterization of PIEZOs, which are unequivocal rapid sensors of mechanical force that apparently evolved specifically for this purpose. The 2021 Nobel Prize for Physiology or Medicine was awarded in part for the discovery of ion channel proteins of this type as sensors of touch, although they have roles in many aspects of biology, functioning as adaptable cassettes in diverse cell types (Beech and Kalli, 2019; Coste et al., 2010; Murthy et al., 2017; Wu et al., 2017) and mediators of various health and disease mechanisms such as red blood cell homeostasis (Zarychanski et al., 2012), malaria resistance (Ma et al., 2018), vascular structure and function (Li et al., 2014), and

lymph edema (Fotiou et al., 2015). They are not the only mechanical sensors. Other ion channels participate as direct sensors or respond indirectly to force via intermediates (Douguet and Honoré, 2019) but also other protein types are implicated (Wyatt et al., 2016), suggesting diverse sensing systems and the detection and tuning of mechanical sensitivity by complex assemblies of proteins, alongside other components such as lipids.

There are two mammalian PIEZO proteins, PIEZO1 and PIEZO2 (Coste et al., 2010; Murthy et al., 2017). They form trimeric ion channels of almost a million Daltons each (Guo and MacKinnon, 2017; Wang et al., 2019). They are molecular machines that almost instantaneously couple mechanical force to transmembrane ion flux (Coste et al., 2010; Wu et al., 2017). They would seem to form only homomeric channels, i.e., trimers of PIEZO1 (PIEZO1 channels) and trimers of PIEZO2 (PIEZO2

[1]Nanion Technologies GmbH, München, Germany; [2]Theoretical Medicine and Biosciences, Saarland University, Homburg, Germany; [3]Experimental Physics, Saarland University, Saarbrücken, Germany; [4]Leeds Institute of Cardiovascular and Metabolic Medicine, School of Medicine, University of Leeds, Leeds, UK.

*N. Murciano and M.G. Rotordam contributed equally to this paper. Correspondence to Markus Rapedius: markus.rapedius@nanion.de; Andrea Brüggemann: andrea@ionchannels.de

channels). They are Ca^{2+}-permeable non-selective cation channels that commonly locate in the plasma membrane, so, when activated, they cause intracellular Ca^{2+} elevations. Measurement of Ca^{2+} events is commonly done for PIEZO1 by applying the small-molecule agonist of PIEZO1 channels, Yoda1 (Evans et al., 2018; Syeda et al., 2015). Yoda1 does not activate PIEZO2 (Syeda et al., 2015) and there are no known equivalents for PIEZO2. One of the physiological mechanical activators of PIEZO1 channels is shear stress (Li et al., 2014; Rode et al., 2017), a frictional force arising when fluid flows along a surface such as a cell membrane. Shear stress has also been seen to stimulate PIEZO1 in Ca^{2+} assays (Li et al., 2014; Maneshi et al., 2018).

Properties of PIEZO channels have, nevertheless, mostly been investigated by the powerful and versatile patch clamp electrophysiology technique used in all of its configurations: whole cell, cell-attached, inside-out, and outside-out excised patches (Coste et al., 2010; Lewis and Grandl, 2015). Several mechanical stimulation (M-Stim) methods have been integrated with the patch clamp. They include mechanical hitting of cells with a stylus and the application of fluid flow to cause shear stress. For membrane patch recordings, rapid on and off pressure pulses are often applied to the patch pipette solution to flex the membrane patch in or out and thereby increase and decrease membrane tension. This is a type of pressure-clamp, somewhat akin to current- and voltage-clamp of the patch clamp method. Pressure-clamp is not, however, a membrane tension clamp, so although the actual tension in the membrane can be estimated, the tension is not absolutely known and may vary in an unknown way during pressure pulses. Regardless of the limitations, these methods have revealed much about the properties of PIEZO channels overexpressed in cell lines, particularly the human embryonic kidney (HEK) 293 cell line. The channels show rapid activation in response to mechanical force and often fast inactivation (a type of desensitization) during sustained force, with slower kinetics at positive voltages (Moroni et al., 2018). Patch clamp has also been used to study native PIEZO channels and it would be valuable to see more such studies because the native channels can behave differently in important regards, for example, showing much slower, or no, inactivation (Evans et al., 2020; Peyronnet et al., 2013; Shi et al., 2020; Del Mármol et al., 2018).

Major technical progress occurred in ion-channel research with the advent of sophisticated automated patch clamp (APC) systems (Obergrussberger et al., 2021), developed primarily to address the needs of chemical screening and small-molecule programs aimed at voltage-gated and ligand-gated ion channels. Several studies have shown the use of high-throughput APC to explore the function and properties of PIEZO1 channels in heterologous expression systems as well as primary cells (Rotordam et al., 2019; Parsonage et al., 2023; Karamatic Crew et al., 2022), mainly based on usage of Yoda1. However, to the best of our knowledge, a combination of pure mechanical activation and high-throughput automated patch has not yet been available for PIEZO1 channels.

Here, we report the mechanical activation of PIEZO1 channels and effects of Yoda1 in a high-throughput APC system and suggest the potential to use such technology to more rapidly advance the understanding of PIEZOs and identify and characterize their small-molecule modulators.

Materials and methods
Cell culture and harvesting
HEK T-REx 293 cells that overexpress human PIEZO1 upon induction with tetracycline were generated as previously described (Rode et al., 2017). Expression was induced by treating the cells for 24 h with 0.5 μg/ml tetracycline (Sigma-Aldrich). HEK T-REx 293 cells that constitutively overexpress murine PIEZO1 were generated as previously described (Blythe et al., 2019). Cells were cultured and harvested according to Nanion's standard protocols (Obergrussberger et al., 2021). Untransfected HEK T-REx 293 cells were used as control cells.

Compounds and recording solutions
For all patch-clamp recordings, the internal solution contained (in mM): 10 KCl, 110 KF, 10 NaCl, 10 EGTA, and 10 HEPES/KOH (pH 7.2), and the external recording solution contained (in mM): 140 NaCl, 4 KCl, 2 $CaCl_2$, 1 $MgCl_2$, 5 glucose, and 10 HEPES/NaOH (pH 7.4). Yoda1 (Tocris) and $GdCl_3$ (Sigma-Aldrich) were dissolved in DMSO and diluted in the external recording solution to a final concentration of 10 and 30, respectively. 0.1% DMSO concentration was used in the external recording solution as a negative control.

APC recordings
Whole-cell patch clamp recordings were conducted on the SyncroPatch 384, a high-throughput patch clamp instrument, according to Nanion's standard procedures (Obergrussberger et al., 2018, 2021). All recordings were performed at room temperature using planar borosilicate glass consumables, the NPC-384 chips.

The SyncroPatch 384 is a 384 well-based system that uses single- or multihole chips (NPC-384) of different resistances (single-hole or 1×, 4–5 MΩ; multihole 0.5–1.3 MΩ). Each well is prepared with 1- (1× chip), 4- (4× chip), or 8- (8× chip) μm-sized apertures and is connected to an individual amplifier channel, thus hosting an individual patch-clamp experiment (Obergrussberger et al., 2021). Cells and solutions are automatically aspirated from different solution reservoirs located at predefined positions and added to the wells by a liquid handling robot (Biomek i5; Beckman Coulter) equipped with 384 pipettes (Fig. 1 A, view of the well from the side). One set of 384 pipettes was used for each experiment; the solution inside the pipettes was replaced at will and the pipettes were washed in between additions (either with water or with solvent and water) to avoid carryover from previous solutions. Cells were captured onto the apertures at the bottom of the wells via negative pressure and were measured at a constant holding potential of –80 mV. To mechanically activate PIEZO1, 20 μl of solution was dispensed at a high flow rate (110 μl/s, unless indicated otherwise) onto the cell(s), in the following called M-Stim, in sync with a triggered recording of 7 s duration, followed by slow (2 μl/s) aspiration to restore the initial volume of 40 μl in each well. In some experiments, different dispense flows of 40, 60, or
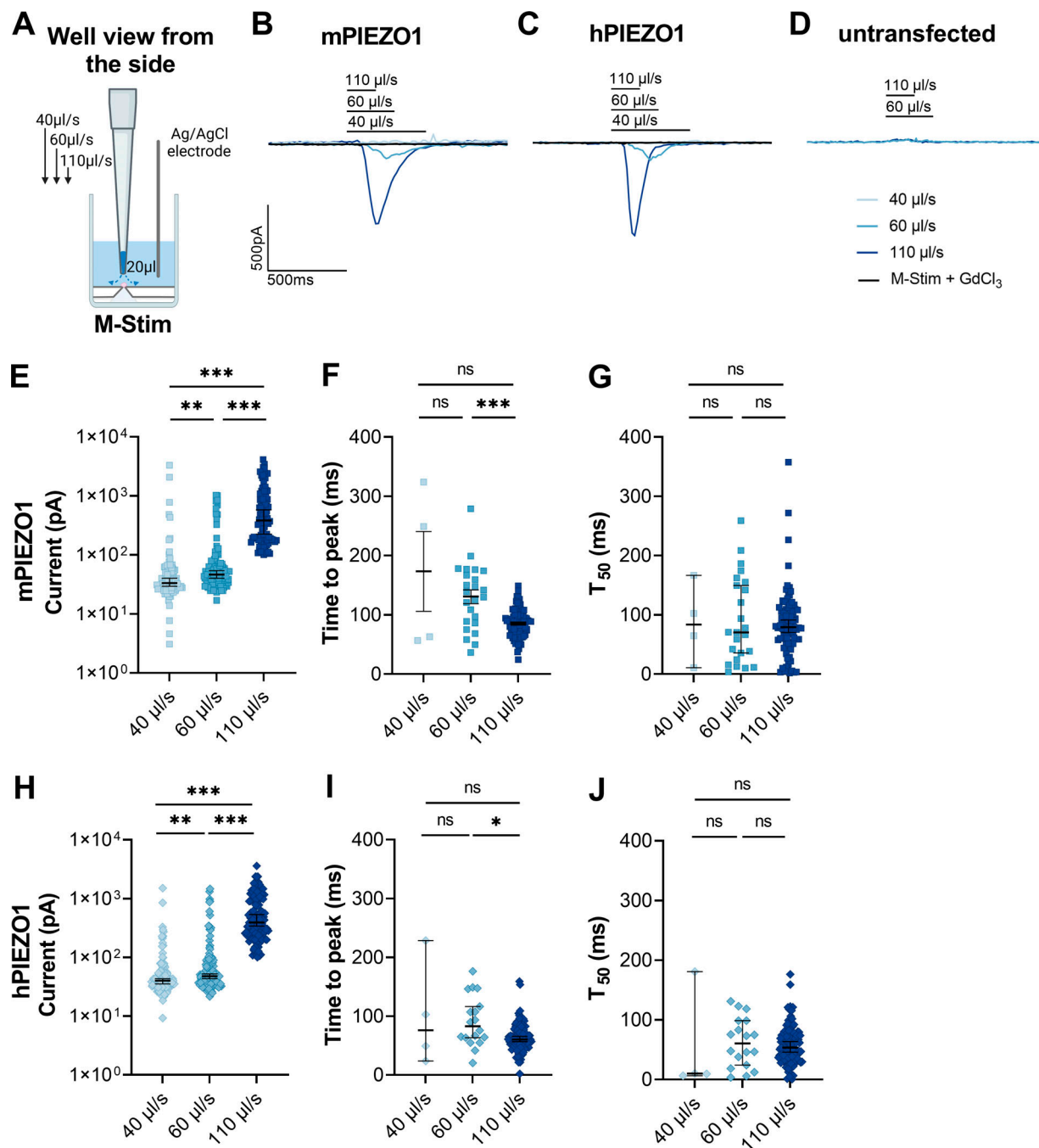
Figure 1. **Mechanical activation of PIEZO1 currents in a high-throughput patch clamp assay. (A)** Schematic illustration of a cross-section of one well of an NPC-384 chip created with BioRender.com. M-Stim was achieved by dispensing 20 µl of solution locally onto the cell (blue dashed arrows) at three different pipetting flows (40, 60, 110 µl/s). **(B–D)** Representative PIEZO1 inward current raw traces of single cells elicited by application of external solution at 40 µl/s (light blue trace), 60 µl/s (blue trace), and 110 µl/s (dark blue trace), and blocked by $GdCl_3$ (black trace) for mPIEZO1 (B), hPIEZO1 (C), and untransfected cells (D). **(E and H)** Absolute peak current amplitudes of mPIEZO1 (E) and hPIEZO1 cells (H) plotted against pipetting flow (mPIEZO1: $n = 123/1,440$; $N = 9$; **$P = 0.007$, ****$P < 0.0001$); hPIEZO1: $n = 123/1,471$; $N = 9$; **$P = 0.02$, ****$P < 0.0001$). **(F, G, I, and J)** Time to peak and T_{50} values (decay time from peak to 50% of the remaining signal) of mPIEZO1 (F and G) and hPIEZO1 cells (I and J) plotted against pipetting flow (mPIEZO1: 40 µl/s $n = 4/1,467$; 60 µl/s $n = 24/1,488$; 110 µl/s $n = 88/1,440$; $N = 9$; hPIEZO1: 40 µl/s $n = 4/1,494$; 60 µl/s $n = 18/1,483$; 110 µl/s $n = 103/1,471$; $N = 9$; ns $P > 0.05$, *$P = 0.02$, ***$P = 0.0006$). All data are shown as values of individual cells with median, and 95% CI indicated in black, tested for statistical significance using a Friedman test (E and H) and Kruskal–Wallis test (F, G, and I) with Dunn's post-hoc test. n represents the number of cells for a given experimental condition out of the total amount of valid cells, and N indicates the number of independent NPC-384 chips.

Murciano et al.
Mechanical activation of Piezo1 channels

Journal of General Physiology   3 of 11
https://doi.org/10.1085/jgp.202213132

110 µl/s were compared, resulting in M-Stim exposure times of the cells of 500, 334, and 182 ms, respectively. The dispense was triggered with a delay of 500 ms from the start of the recording protocol. All currents were blocked by 30 µM GdCl$_3$ that was dispensed at the maximum speed of 110 µl/s to the cells, after a preincubation time of 40 s.

In the experiments testing the effect of dispense speed, each cell received 3× M-Stim additions (1× for each dispense speed) followed by 3× M-Stim + Yoda1 additions (1× for each dispense speed), hence a total of six consecutive liquid puff applications. In multihole chip experiments, each cell received 3× or 4× M-Stim additions followed by 1× M-Stim + Yoda1 addition, all dispensed at 110 µl/s. Whenever multiple identical M-Stim additions were applied, the current amplitude stabilized within three M-Stim additions, hence only the last one was considered for the analysis (see Fig. S3 and Table S3).

For each set of experiments, the absolute current amplitude, the activation and inactivation time course of the currents, and the percentage of responsive wells (% responders), assessed according to our quality control criteria (see Quality control parameters), were evaluated. The analysis of the activation and inactivation time courses was assessed by the time to reach the minimum current at peak (time to peak) and the time from peak to 50% of the remaining signal with respect to the unstimulated baseline current (T$_{50}$). T$_{50}$ provides an approximation of the decay of the PIEZO1-mediated currents; however, in our experimental setting, it is of limited validity for characterizing the inactivation time course of PIEZO1 signals since our stimulation is stopped after the application of 20 µl at the different dispense flows used.

Mechanical effects of M-Stim

The mechanical effects generated by the M-Stim approach can be accounted for by two processes, direct pressure (1) and shear stress (2) acting on the cell. In all recordings conducted for this study, we used flow rates (Q) prearranged by the robot provider (Beckman Coulter) of 40, 60, or 110 µl/s, in conjunction with Biomek i-Series tips (50 µl, non-sterile, product no. B85753) having an inner tip diameter of 300 µm at the outlet. The pipette tip was fixed at a position of 1 mm from the cell and directed above the center of the cell for 1× chips, and in the middle of the array for 4× and 8× chips, as indicated in Fig. 1 A, Fig. 2 A, and Fig. S1.

(1) Using the impinging jet theory, the pressure can be assessed through Bernoulli's equation:

$$P = \frac{\rho v^2}{2},$$

where ρ is the fluid density assumed to be equal to that of water (ρ = [10^3 kg]/m^3) and v is the flow velocity, calculated as v = 4Q/πD^2, with D = 300 µm (standard orifice diameter of Biomek i-Series tips).

The maximum pressure exerted at the central position of the pipette tip is 1,600, 3,600, or 12,000 dyn/cm^2 for the flow rates Q of respectively 40, 60, or 110 µl/s, and drops by 10% toward the edge of the inner tip diameter, i.e., there is no big difference whether a 1× chip, a 4× chip, or an 8× chip is used.

(2) The shear stress can be computed through the Hiemenz's solution:

$$\tau = \frac{1.873}{2} \sqrt{\eta\rho} \left(\frac{v}{D}\right)^{3/2} r,$$

where r is the radial position from the center of the pipette (Tu and Wood, 1996) and η = 10^{-3} Pa.s. In an idealistic scenario, the shear stress applied in the middle of a single-cell centered under the pipette is thus always zero (r = 0). However, at the edge of such a single cell (r = 10 µm) for the flow rates Q of 40, 60, and 110 µl/s, the shear stress τ is 7.8, 14, and 35 dyn/cm^2, respectively.

In contrast, at the center of the cells of the 4× chip with a centered pipette (r = 70 µm), one obtains shear stresses τ of respectively 55, 100, and 250 dyn/cm^2.

The maximum shear stress that a cell could sustain observed under the edge of the pipette (r = D/2 = 150 µm) is 120, 210, and 530 dyn/cm^2, respectively. This means for the highest flow rate of 110 µl/s, the shear stress for a cell on a 1× chip could be in the range of 35 dyn/cm^2 at the edge of the cell to 530 dyn/cm^2 whereas, for 4× chips, this range is 250–530 dyn/cm^2.

Quality control parameters

All cells with seal resistance above 0.3 GΩ throughout the experiment were considered valid cells for the analysis. Next, we identified PIEZO1 responding wells as those with peak current amplitudes >100 pA in M-Stim and M-Stim + Yoda1 conditions. To detect and eventually remove artefactual responses from the analysis, we assessed the area under the curve parameter per each cell and accepted values exceeding < –20 pA·s. These criteria were set as quality control filters in the recording software (PatchControl 384; Nanion Technologies GmbH) for online analysis and automated cell selection during the experiment.

Data analysis

DataControl384 (Nanion Technologies GmbH) and Prism 9 (GraphPad Software) were used for all analyses. Data are presented as median with 95% CI, being non-normally distributed according to the Shapiro-Wilk test. Throughout the manuscript, n represents the number of responding wells for a given experimental condition out of the total amount of valid wells and N indicates the number of independent NPC-384 chips. The signals of 9–25% of responding wells could not be used for kinetic analysis due to inappropriate fitting parameters. To assess statistical power of non-normally distributed data, Mann-Whitney tests were used for comparisons between two sets of data, and Kruskal-Wallis ANOVA with Dunn's post-hoc tests were used for comparisons within different conditions of the same dataset. One-way ANOVA was used with Tukey's post-hoc test for normally distributed data. P < 0.05 was deemed significant. Exact P values are indicated within the figure legends.
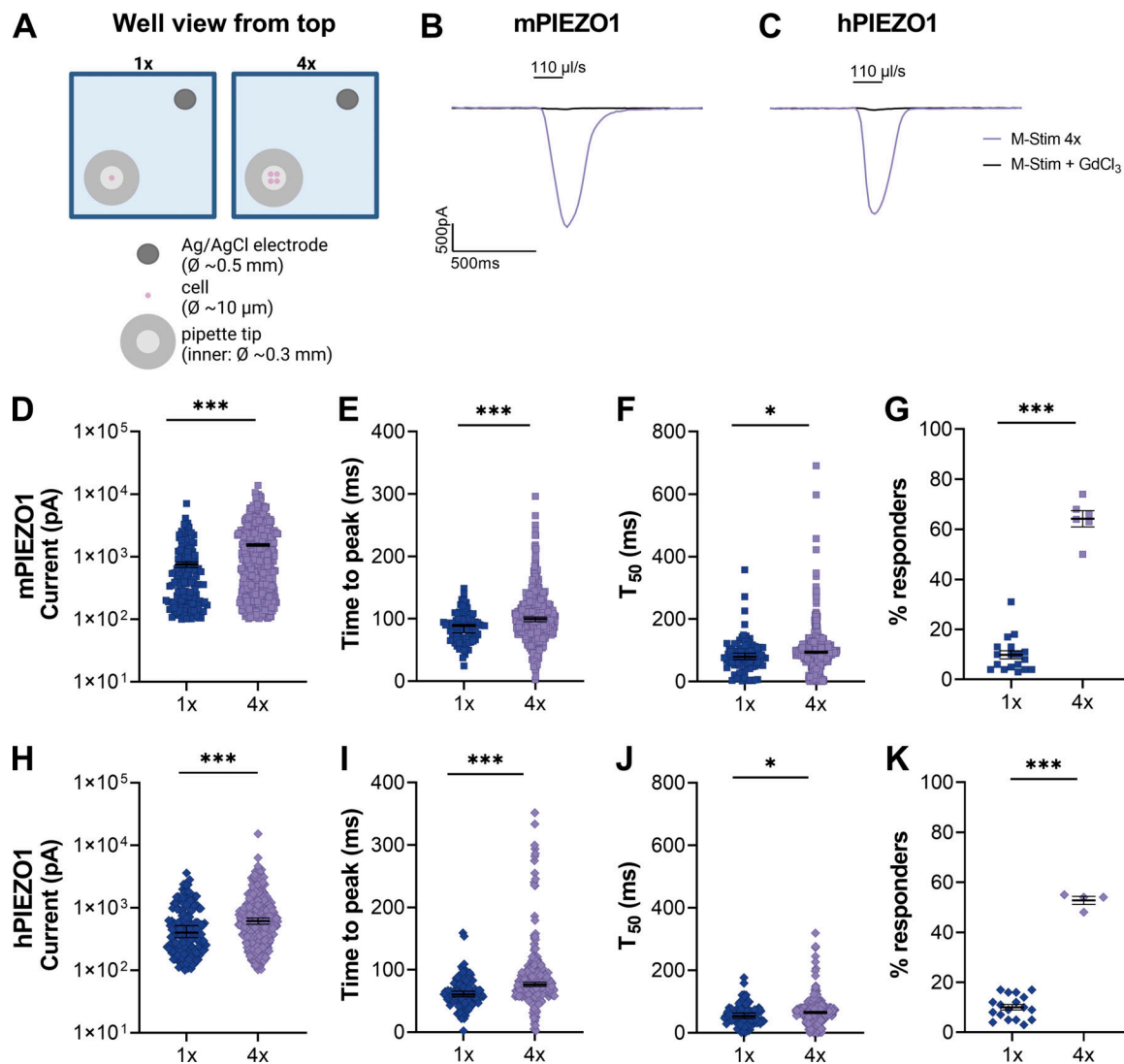
Murciano et al.
Mechanical activation of Piezo1 channels

Journal of General Physiology
https://doi.org/10.1085/jgp.202213132

4 of 11

Figure 2. **Increased current read-out upon M-Stim using multihole chips. (A)** Schematic illustration of the top view of one well of an NPC-384 chip with one patch hole (left) and four patch holes (right) created with BioRender.com. **(B and C)** Representative mPIEZO1 (B) and hPIEZO1 (C) inward current raw traces recorded from a 4× chip elicited by M-Stim at 110 µl/s. **(D and H)** Absolute current values of mPIEZO1 (D) and hPIEZO1 (H) cells recorded from single-hole chips (1×, dark blue) and four-hole chips (4×, purple) (mPIEZO1: 1×, n = 148/1,910; N = 18; 4×, n = 579/941; N = 6; hPIEZO1: 1×, n = 174/1,919; N = 18; 4×, n = 346/667; N = 4; ****P < 0.0001). **(E, F, I, and J)** Time to peak and T_{50} values (decay time from peak to 50% of the remaining signal) of mPIEZO1 (E and F) and hPIEZO1 cells (I and J) recorded from 1× (dark blue) and 4× (purple) chips (mPIEZO1: 1×, n = 88/1,440; N = 9; 4×, n = 506/843; N = 5; *P = 0.02, ****P < 0.0001; hPIEZO1: 1×, n = 103/1,471; N = 9; 4×, n = 324/667; N = 4; *P = 0.04, ****P < 0.0001). **(G and H)** Percentage of mPIEZO1 (G) and hPIEZO1 (H) wells responding to activation by M-Stim at 110 µl/s pipetting flow using 1× (dark blue) and 4× (purple) chips (mPIEZO1: 1×, N = 18; 4×, N = 6; hPIEZO1: 1×, N = 18; 4×, N = 4; ****P < 0.0001). **(K)** Data are shown as values of individual cells with median, and 95% CI (D–F and H–J), or as mean ± SEM (G and K), indicated in black, tested for statistical significance Mann-Whitney test and unpaired t test. n represents the number of cells for a given experimental condition out of the total amount of valid cells, and N indicates the number of independent NPC-384 chips.

Online supplemental material

Fig. S1 displays example raw traces, current amplitudes, activation/decay time courses of mPIEZO1 signals, and the fraction of responding wells obtained from 8× chips in comparison to 1× and 4× chips. Fig. S2 shows example raw traces and current amplitudes of endogenous PIEZO1 signals and a fraction of responding wells obtained from untransfected cells using 1× and 4× chips. Fig. S3 provides information on the repeatability of PIEZO1 currents over multiple M-Stim additions. Supplemental tables compare the properties of mechanically activated signals elicited from mPIEZO1 and hPIEZO1 in various conditions (Table S1), endogenous PIEZO1 from untransfected cells (Table S2), and mPIEZO1 and hPIEZO1 by four identical M-Stim applications (Table S3).

Results

High-throughput APC method to assess mechanical activation of PIEZO1 currents

To stimulate PIEZO1 channels mechanically in a high-throughput patch clamp assay, HEK293 cells overexpressing murine or human PIEZO1 (mPIEZO1 and hPIEZO1, respectively)

Murciano et al.
Mechanical activation of Piezo1 channels

Journal of General Physiology 5 of 11
https://doi.org/10.1085/jgp.202213132

and untransfected HEK293 cells were transiently exposed to small amounts or "puffs" of liquid (external solution, 20 µl) dispensed at fast pipetting speeds on top of the cell by robotic pipettes used to serve the 384 individual wells of the Syncro-Patch 384 (Fig. 1 A). This directed solution flow was intended to cause mechanical forces to act on the cell membrane with effective pressure scaling with increasing pipetting flows. In the following, the fast dispensing of solution directly onto the cell will be referred to as mechanical stimulation or M-Stim.

To evaluate if liquid puffs are suited to mechanically stimulate PIEZO1 channels, mPIEZO1, hPIEZO1, and untransfected cells were measured simultaneously in one NPC-384 chip and exposed to M-Stim at three different pipetting flows, 40, 60, and 110 µl/s. Upon M-Stim application, we observed fast activating and fast decaying currents from mPIEZO1 and hPIEZO1 cells that were blocked by $GdCl_3$, a known inhibitor of cationic mechanosensitive currents (Fig. 1, B and C; Coste et al., 2010). These currents were absent in untransfected cells under the same conditions, hinting that M-Stim elicited PIEZO1-mediated responses (Fig. 1 D). To assess the impact of the pipetting flow on the stimulation of PIEZO1 channels, we selected a subset of cells activated by M-Stim at 110 µl/s and compared their peak current amplitudes in response to the three different application flows. At 110 µl/s, the median current amplitude was −382 pA for mPIEZO1 and −391 pA for hPIEZO1, significantly higher compared with the values obtained at 60 µl/s (−46 pA for mPIEZO1 and −48 pA for hPIEZO1) and 40 µl/s (−33 pA for mPIEZO1 and −40 pA for hPIEZO1) from the same cells ($n = 96/1,440$, $N = 9$ for mPIEZO1; $n = 123/1,471$, $N = 9$ for hPIEZO1; Fig. 1, E and H). To further characterize the effect of the pipetting flow, and hence the pressure exerted, we identified the responding wells over the total wells considered for the analysis (for the definition of responding wells, see Materials and methods) for each pipetting flow to describe the activation and the decay time courses of the currents. The time to peak was significantly shorter at 110 µl/s, with a minimum of 88.5 ms ($n = 88/1,440$, $N = 9$) for mPIEZO1 (Fig. 1 F) and of 60.4 ms ($n = 103/1,471$, $N = 9$) for hPIEZO1 (Fig. 1 I), compared with 60 µl/s (134.3 ms, $n = 24/1,458$, $N = 9$ for mPIEZO1, Fig. 1 F; 83 ms, $n = 18/1,483$, $N = 9$ for hPIEZO1, Fig. 1 I) but not to 40 µl/s, probably due to the limited number of cells activated by M-Stim and the high variability of the time to peak values at that speed. In contrast, our data at 110 µl/s show a smaller variance and less scattered data points relative to the median compared with lower application flows, specifically for time to peak (Table S1). For the time course of current decay (T_{50}), we observed no significant differences both for mPIEZO1 (Fig. 1 G) and hPIEZO1 (Fig. 1 J) at the three different pipetting flows used, probably due to the signal decay coinciding with the end of the liquid puff/force application. However, at 110 µl/s, hPIEZO1 showed 1.5-fold smaller values for time to peak and T_{50} compared to mPIEZO1 (Table S1), suggesting differences between mPIEZO1 and hPIEZO1 with respect to the time course of channel opening and closure. Taken together, these results indicate that fast pipetting flow (110 µl/s) is a key factor for the mechanical activation of PIEZO1 channels on the SyncroPatch 384.

Increasing the current read-out of the M-Stim approach using multihole chips

To obtain larger current amplitudes per well, multihole chips can be used to record the sum of the currents of multiple cells on one electrode, improving the signal-to-noise ratio. As such, the use of multi-hole chips is a standard tool in the assay development of APC experiments to improve efficiency. To increase the current amplitudes and the fraction of responding wells in the M-Stim approach, we employed multi-hole chips to record PIEZO1 currents of four or eight cells per well (Figs. 2, S1, and S3) using 110 µl/s application speed. With the array of holes (four or eight) centered under the aperture of the pipette tip, M-Stim results in synchronous stimulation of the cells. When applying M-Stim on four cells per well simultaneously, we observed a significant increase in the peak current amplitudes from −388 pA (1×, $n = 148/1,910$, $N = 18$) to −894 pA (4×, $n = 579/941$, $N = 6$) for mPIEZO1 and from −399 pA (1×, $n = 174/1,919$, $N = 18$) to −613 pA for hPIEZO1 (4×, $n = 346/667$, $N = 4$; Fig. 2, B–D and H). Under identical experimental conditions, the current response to M-Stim of untransfected cells was low with a median of −256 pA, and only 29 of 485 cells qualified for analysis (for definition of responding wells, see Materials and methods section), consistent with the reports that expression of endogenous PIEZO1 channels may confound the results in HEK293 cells (Dubin et al., 2017; Fig. S2, A and B; and Table S2). For mPIEZO1 in 4× chips, the fraction of wells with current responses above the threshold increased significantly from 9.8 ± 1.6% (1×, $n = 148/1,910$, $N = 18$) to 64.2 ± 3.2% (4×, $n = 579/941$, $N = 6$) and for hPIEZO1 from 10 ± 1.1% (1×, $n = 174/1,919$, $N = 18$) to 52.7 ± 1.6% (4×, $n = 346/667$, $N = 4$; Fig. 2, G and K). In contrast, for untransfected cells, a significantly lower ($P < 0.0001$) number of cells qualified as responders with 0.7 ± 0.3% (1×, $n = 3/432$, $N = 9$) and 5.8 ± 2% (4×, $n = 29/485$, $N = 5$), suggesting a rather low contribution of endogenous PIEZO1 during M-Stim additions (Fig. S2, A and B; and Table S2). Interestingly, the use of 8× chips did not further increase the current amplitude and fraction of wells responding above the threshold (Fig. S1, D and G), indicating that M-Stim on 4× chips constitutes the optimal approach for the study of PIEZO1 channels on the SyncroPatch 384. However, 4× chips displayed a significantly slower activation time course of PIEZO1 signals than 1× chips, with a time to peak of 99.5 ms (4×, $n = 506/941$, $N = 6$) compared with 88.5 ms (1×, $n = 88/1,440$, $N = 9$) for mPIEZO1 (Fig. 2 E) and 76.3 ms (4×, $n = 324/667$, $N = 4$) compared with 60.4 ms (1×, $n = 103/1,471$, $N = 9$) for hPIEZO1 (Fig. 2 I). The same applies to the time course of current decay, being overall slower in 4× than 1× chips, with median T_{50} values of 94.6 ms (4×, $n = 506/941$, $N = 6$) versus 79.3 ms (1×, $n = 88/1,440$, $N = 9$) for mPIEZO1 (Fig. 2 F) and of 64.1 ms (4×, $n = 324/667$, $N = 4$) versus 53.4 ms (1×, $n = 103/1,471$, $N = 9$) for hPIEZO1 (Fig. 2 J). Overall, when comparing the two clones, stimulation of mPIEZO1 resulted in significantly higher peak currents compared with hPIEZO1 (Table S1), while values of time to peak and T_{50} confirm that hPIEZO1 currents are faster activating as well as decaying compared with mPIEZO1 ones, as previously observed with 1× chips (Table S1).

Murciano et al.
Mechanical activation of Piezo1 channels

Journal of General Physiology
https://doi.org/10.1085/jgp.202213132

6 of 11

Evaluation of the M-Stim approach in the presence of Yoda1

To investigate small-molecule modulation in the newly developed M-Stim approach, we combined it with Yoda1 (M-Stim + Yoda1), a small molecule lowering the threshold for PIEZO1 mechanical activation (Syeda et al., 2015; Botello-Smith et al., 2019), which was added at 10 µM concentration to the external solution in the liquid puff approach (Fig. 3 A). Again, M-Stim + Yoda1 was tested on mPIEZO1, hPIEZO1, and untransfected cells in parallel in one NPC-384 chip at 40, 60, and 110 µl/s application speeds for a direct comparison with M-Stim only. As with M-Stim only, increasing the dispense speed with M-Stim + Yoda1 resulted in significantly higher peak currents for mPIEZO1 and hPIEZO1 (Fig. 3, B–E, and I), thus confirming the suitability of our M-Stim approach for the study of PIEZO1 channels when increasing pipetting flow. Moreover, in 1× conditions, the current onset was faster at 110 µl/s compared with lower pipetting flows, with a time to peak of 97.2 ms for mPIEZO1 (Fig. 3 F) and 83.2 ms for hPIEZO1 (Fig. 3 J). In addition, T_{50} significantly decreased with increasing flows, from 173 ms ($n = 141/1,420$) at 40 µl/s to 92.5 ms at 110 µl/s ($n = 465/1,353$) for mPIEZO1 ($N = 9$, Fig. 3 G), and from 158 ms ($n = 104/1,425$ at 40 µl/s to 72 ms ($n = 460/1,390$) at 110 µl/s for hPIEZO1 ($N = 9$, Fig. 3 K). However, the activation/decay time courses of the currents were overall slower (<1.4-fold) than the ones obtained using M-Stim alone, indicating the anticipated effects of Yoda1 as a gating modifier of PIEZO1 channels upon M-Stim (Syeda et al., 2015). Compared with M-Stim only, M-Stim + Yoda1 in 1× chips enhanced the number of responding wells by approximately fourfold (43.9 ± 3.7%, $n = 693/1,785$, $N = 18$, Fig. 3 H) for mPIEZO1 and threefold (36.3 ± 2.5%, $n = 637/1,832$, $N = 18$, Fig. 3 L) for hPIEZO1. Moreover, a direct comparison of the two clones showed that M-Stim + Yoda1 elicited significantly larger current amplitudes from mPIEZO1 than from hPIEZO1, the latter with a 1.2-fold faster signal onset and a 1.3-fold faster signal decay (Table S1).

M-Stim + Yoda1 proved to be a more efficient approach for studying PIEZO1, especially in combination with multihole chips. In fact, using 4× chips improved the success rate by increasing peak currents (−4.7 nA, $n = 685/722$, $N = 6$, for mPIEZO1, Fig. 3 E; −3.2 nA, $n = 577/604$, $N = 4$, for hPIEZO1, Fig. 3 I) and yielding a higher fraction of wells with current amplitudes above threshold (>95% in both clones) compared with 1× chips (Fig. 3, H and L). However, under these experimental conditions, we observed a notable current response from untransfected cells and the fraction of responding wells increased significantly from 4% (M-Stim only) to 19% upon M-Stim + Yoda1 addition. Yet, with −234 pA ($n = 82/448$; $N = 5$), the median current was at least 13-fold smaller (P > 0.0001) compared with both overexpressed channels, further confirming a low contribution of endogenous PIEZO1 in our approach (Fig. S2, B and C; and Table S2), and in line with previous reports (Bae et al., 2013a; Dubin et al., 2017). While 8× chips resulted in a further increase of the median current amplitude at 110 µl/s in mPIEZO1, reaching −6.7 nA ($n = 2,425/2,459$, $N = 10$, Fig. S1 H), the fraction of wells with current amplitudes above threshold did not increase significantly (Fig. S1 K). Similar to M-Stim only, the activation/decay time courses were slower (<1.5-fold) for 4×

(and 8×, Fig. S1, I and J) compared with 1× chips at the same pipetting flow (Fig. 3, E, F, I, and J). However, when comparing the two clones in 4× chip conditions, hPIEZO1 elicited significantly smaller currents than mPIEZO1 but showed faster (<1.5-fold) activation/decay time courses, which is consistent with the result we observed for M-Stim alone (Fig. 2).

Taken together, these results confirm that 4× chips combined with M-Stim (±Yoda1) are a valuable tool for the study of PIEZO1 channels on SyncroPatch 384.

Discussion

In this study, we set out to develop a high-throughput approach to mechanically stimulate cells expressing the mechanosensitive ion channel PIEZO1, while recording current responses from individual cells. To this end, we used the SyncroPatch 384, a high-throughput APC device, employing high-speed solution application for M-Stim while recording triggered current responses from 384 cells in parallel. Originally designed for eliciting fast-activating currents from ligand-gated channels (Obergrussberger et al., 2022), this approach was adapted to the investigation of mechanosensitive channels like PIEZO1 when higher dispense speeds of up to 110 µl/s became available with the new SyncroPatch 384 system compared with a maximum of 40 µl/s in the predecessor model of the SyncroPatch 384. To optimize the mechanosensitive current response, we focused on two parameters: the pipetting speed of the solution applied onto the cell surface and the number of holes/cells per well. To determine the optimal configuration of these parameters, we analyzed the peak current amplitude, the fraction of cells showing a PIEZO1 current response, and the activation/decay time courses of the current response.

The pipetting flow of the applied solution is the key parameter determining the force impinging upon the cell membrane. We modified the pipetting flow by comparing three different settings, 40, 60, and 110 µl/s, with the highest flow eliciting up to 11-fold larger current amplitudes and being up to 50-fold more effective at evoking mechanosensitive current responses above the threshold than the lower pipetting speeds, both for mPIEZO1 and hPIEZO1. Moreover, the time to peak velocity was significantly increased when scaling from 60 to 110 µl/s, in line with a higher pressure acting on the cells. There was no speed-dependent difference in T_{50} values for mPIEZO1 and hPIEZO1, likely due to the stopping of the M-Stim application preceding or coinciding with the decay phase of the channel. However, at the highest pipetting flow, hPIEZO1 signals showed faster activation and decay time courses of the currents compared with mPIEZO1, consistent with previous findings obtained via poking or pressure clamp stimulations (Coste et al., 2010, 2012; Bae et al., 2013b). This finding provides a good indication that our approach can differentiate between two clones, and, to our best knowledge, this study is one of the first to report on a systematic comparison of both clones expressed in HEK293 cells.

To increase the efficiency of our approach, we used multihole chips having four or eight holes per well (Fig. 2 and Fig. S1). The array of the holes was centered under the pipette tip, thus allowing for synchronous activation of the cells by our M-Stim
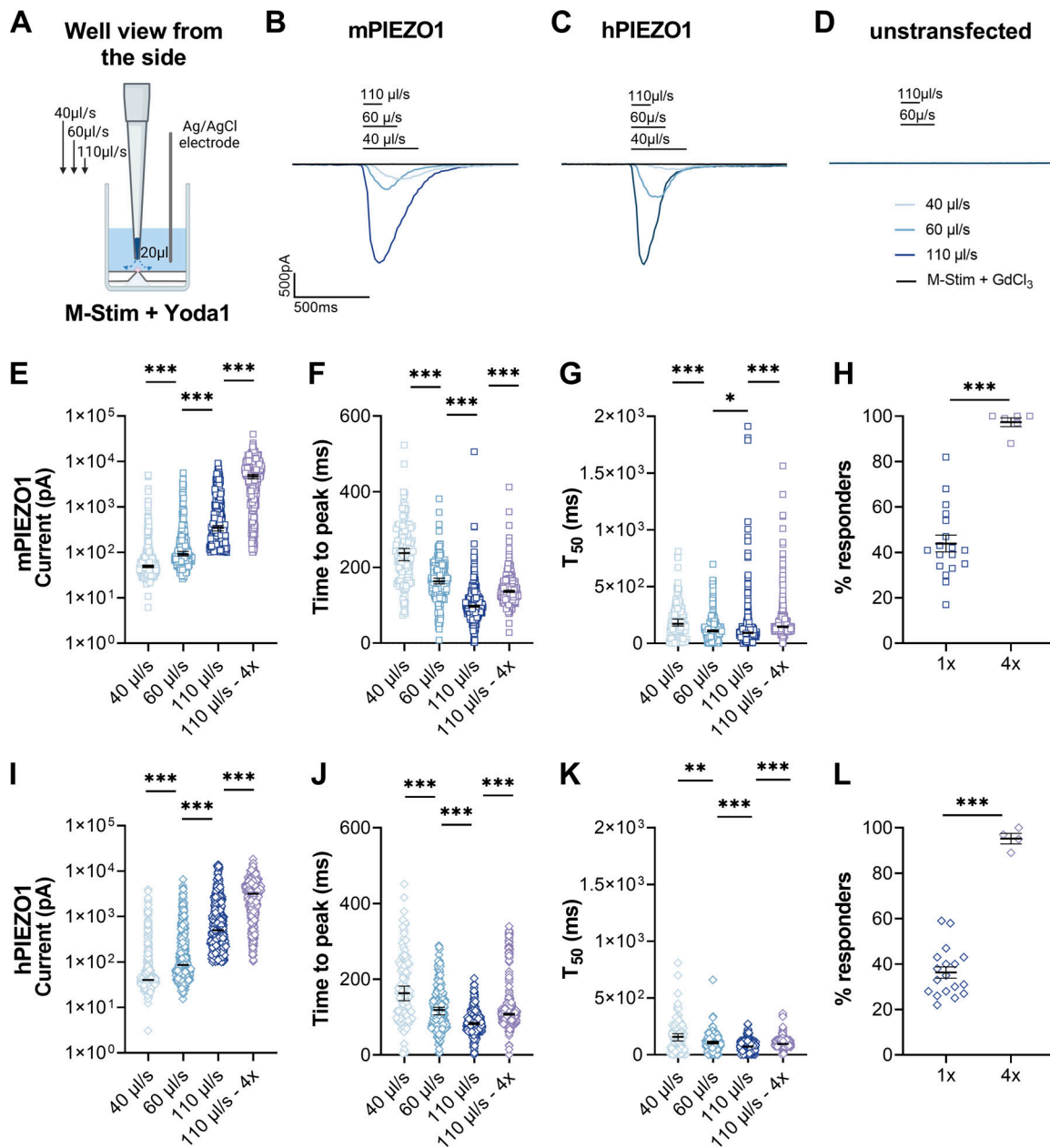
Figure 3.   **Evaluation of the M-Stim approach in the presence of Yoda1. (A)** Schematic illustration of a cross-section of one well of an NPC-384 chip as in Fig. 1 A created with BioRender.com. **(B–D)** Representative PIEZO1 inward current raw traces of single cells elicited by application of 20 µl of 10 µM Yoda1 at 40 µl/s (light blue trace), 60 µl/s (blue trace), and 110 µl/s (dark blue trace), and blocked by $GdCl_3$ (black trace) for mPIEZO1 (B), hPIEZO1 (C) and untransfected cells (D). **(E and I)** Absolute peak current amplitudes elicited by M-Stim + Yoda1 of mPIEZO1 (E) and hPIEZO1 (I) cells plotted against pipetting flow (mPIEZO1: 1×, $n = 465/1,353$; $N = 9$; 4×, $n = 685/722$; $N = 6$; hPIEZO1: 1×, $n = 456/1,390$; $N = 9$; 4×, $n = 577/604$; $N = 4$; ****$P < 0.0001$). **(F, G, J, and K)** Time to peak and T_{50} values (decay time from peak to 50% of the remaining signal) of mPIEZO1 (F and G) and hPIEZO1 (J and K) cells plotted against pipetting flow (mPIEZO1: 1×, 40 µl/s $n = 142/1,420$; 60 µl/s $n = 242/1,388$; 110 µl/s $n = 465/1,353$; $N = 9$; 4×, 110 µl/s $n = 662/697$; $N = 5$; *$P = 0.02$, ****$P < 0.0001$; hPIEZO1: 1×, 40 µl/s $n = 104/1,425$; 60 µl/s $n = 227/1,412$; 110 µl/s $n = 566/604$; *$P = 0.009$, ****$P < 0.0001$). **(H and L)** Percentage of mPIEZO1 (H) and hPIEZO1 (L) wells responding to activation by M-Stim + Yoda1 at 110 µl/s pipetting flow recorded from 1× (dark blue) and 4× (purple) chips (mPIEZO1: 1×, $N = 18$; 4×, $N = 6$; hPIEZO1: 1×, $N = 18$; 4×, $N = 4$, ****$P < 0.0001$). Data are shown as values of individual cells with median and 95% CI (E–G and I–K), or as mean ± SEM (H and L), indicated in black, tested for statistical significance using Kruskal–Wallis test with Dunn's post-hoc test and unpaired t test. n represents the number of cells for a given experimental condition out of the total amount of valid cells, and N indicates the number of independent NPC-384 chips.

approach. When using 4× chips, we increased the fraction of responding wells by 6/7-fold, and the current amplitudes only by 1.5/2-fold—not 4-fold—compared with 1× chips, probably due to the recruitment of more cells above the threshold, leading to a broader distribution of current amplitudes and a shift of the median toward lower amplitudes. The same reasoning applies to 8× chips measurements, where we did not observe an improvement in the success rate. The activation and decay time courses of the currents were up to 1.5-fold slower in multihole chips, likely due to variations in the response times of individual

cells in one well. Among the multihole chips, 8× chips require a slightly higher cell density compared to chips with four or one hole(s) per well; however, their usage is relevant for enhancing the response of cells with poor current read-out. Since the M-Stim approach elicited current amplitudes of comparable size between 4× and 8× chips (Fig. S1 D), using 4× chips constitutes the most efficient approach according to our study.

Our data demonstrates that a combination of fast pipetting together with the use of 4× chips represents an effective tool to evoke PIEZO1 current responses by M-Stim (mPIEZO1 64.2 ± 3.2%; hPIEZO1 52.7 ± 1.6%) without any chemical aid. If a higher success rate is needed, we recommend combining the M-Stim approach with the application of Yoda1 (mPIEZO1 97.3 ± 1.9%; hPIEZO1 95.2 ± 2.5%).

Of note, caution must be taken in the selection of the expression system given the presence of endogenous PIEZO1 currents in HEK293 cells, particularly when the expression levels of the overexpressed constructs are low. In line with previous studies (Bae et al., 2013a; Lukacs et al., 2015; Dubin et al., 2017), we detected low-amplitude endogenous PIEZO1 currents in a small fraction of untransfected HEK293 cells, indicating that their proportion in mPIEZO1 and hPIEZO1 overexpressing cells is negligible. However, the combination of a mechanically nonresponsive background as previously described (Dubin et al., 2017) together with stable expression of PIEZO1 represents an unbiased opportunity to study PIEZO1 regardless of its endogenous expression levels.

A stimulus-dependent activation of mechanosensitive currents, e.g., faster and larger currents, has also been observed when endogenously and heterologously expressed PIEZO1 channels were mechanically stimulated using either a pressure clamp device or a poking probe (Coste et al., 2010; Lacroix et al., 2018; Wijerathne et al., 2022). The M-Stim approach resulted in ~17-fold slower activation kinetics than poking (mPIEZO1: 4.9 ms, Peralta et al., 2023) and ~2/5-fold slower inactivation kinetics (at –80 mV holding potential) than poking (mPIEZO1: 16 ms, Coste et al., 2010) or pressure clamp (mPIEZO1: 48 ms, Lacroix et al., 2018), respectively. In particular, the time course of activation is relatively slow compared to other approaches which suggests that the M-Stim approach is less effective, eliciting most likely non-saturating current responses, even at the maximum flow setting. Furthermore, we cannot rule out the involvement of indirect mechanisms (such as via second messenger systems or the status of cytoskeleton interactions) that could contribute to the pathway of activation in M-Stim and might explain the differences in kinetics observed. Nevertheless, our M-Stim approach did elicit a stimulus-dependent activation with faster and larger currents using elevated pipetting flows, and the time courses observed were significantly different between h- and mPIEZO1 in the absence and presence of Yoda1.

Unfortunately, the adjustment in pipetting parameters for the liquid handling robot is limited to a maximum of 110 μl/s, and therefore we could not test faster flow settings for solution additions in these experimental conditions.

To comprehend the stimuli acting on the cell membrane in our M-Stim approach, we considered two main mechanical processes acting on the cell(s): direct pressure (i.e., stretch/compression) and shear stress, and a combination of both processes can be probably accounted for eliciting PIEZO1 currents in M-Stim. We speculate that the contribution of each process is different between 1× chips, where the center of the pipette tip is aligned with the patch clamp aperture/cell versus multihole chips, where the pipette tip is aligned with the center of the patch clamp apertures/cells' array. When evaluating the stretch/compression component of the mechanical stimuli, Coste et al. (2010) reported that a pressure of –31.2 mmHg, corresponding to ~41,600 dyn/cm², is required for half-maximal activation of PIEZO1 channels in cell-attached configuration from overexpressing HEK293 cells. In our setup, we could not reach such elevated pressure values and it is not clear whether these would be sufficient to elicit PIEZO1-mediated currents as we performed all measurements in whole-cell configuration, i.e., pressure was not exerted on an intact cell membrane. As for the second component, according to Ranade et al. (2014), a shear stress of 52–64 dyn/cm² is required to activate PIEZO1 channels from overexpressing HEK293 cells. In our M-Stim approach, we estimated the contribution of the shear stress ranging from 0 to 35 dyn/cm² at 110 μl/s in 1× chips and being 7-fold higher in 4× compared to 1× chips, which may very well explain why we observed a 6/7-fold lower fraction of responding wells in 1× chips. Based on Tu and Wood (1996), we also estimated that in the case of suboptimal pipette-cell alignment, such as under the edge of the pipette tip (D = 150 μm, see Materials and methods), the shear stress could increase to reach a maximum of 530 dyn/cm² independent on the number of cells composing the array. Here, slight and uncontrollable manufacturing variations of the consumables used (pipette tips, chips) may also affect the pipette-cell alignment and since we lack optical access to our M-Stim approach, we are not able to explore how the pressure translates into current activation in detail. Taken together, these findings might explain why we did not observe major differences between 4× and 8× chips in our study. Nevertheless, these variations seem not to be a rate-limiting factor for the activation of mPIEZO1- and hPIEZO1-mediated currents by M-Stim.

When comparing our approach with other techniques, another crucial difference is that the planar patch clamp technology requires cells to be in suspension as a starting point for the measurement (as described in Materials and methods), which deviates from manual patch clamp studies where cells are usually attached to a coverslip. The different states of the cellular organization (e.g., cytoskeleton arrangements, the composition of the lipid bilayer) may have an impact on the mechanical sensitivity of PIEZO1 channels (Nourse and Pathak, 2017; Shi et al., 2020) and thus could affect the variability in responses and might also contribute to the fact that a different range of shear stress is needed to activate PIEZO1 currents in our M-Stim approach.

To maximize the efficiency of our M-Stim approach, we combined it with the small molecule Yoda1 (Syeda et al., 2015). Yoda1 is to date one of the most effective tools to investigate PIEZO1 channels as it lowers the force needed to mechanically activate the channels (Syeda et al., 2015; Botello-Smith et al., 2019). We also used Yoda1 combined with an APC assay in previous reports to study a novel PIEZO1 mutation in red blood cells (Rotordam et al., 2019) to evaluate the efficacy of potential Yoda1 analogs (Parsonage et al., 2023) and to help to characterize

PIEZO1 channels in the Er-antigen blood group system (Karamatic Crew et al., 2022).

Replacing the external solution with Yoda1 as a liquid puff in the pipette resulted in increasing the fraction of responding wells by up to 5-fold in 1× conditions and up to 1.8-fold in 4× conditions (for both clones), as expected based on the properties of the compound (Syeda et al., 2015). Moreover, Yoda1 slowed down activation and decay time courses of the currents by up to 1.3-fold, consistent with stabilizing the PIEZO1 open state upon M-Stim (Syeda et al., 2015; Lacroix et al., 2018; Wijerathne et al., 2022). Comparing both clones, hPIEZO1 showed a faster onset and decay of over mPIEZO1 signals, thus confirming the findings obtained with M-Stim only (Table S1) and M-Stim + KC159 (Parsonage et al., 2023), suggesting potential differences in the kinetics of channel opening/closure for both clones. At maximum pipetting flow, M-Stim + Yoda1 yielded five- and eightfold larger current responses than M-Stim alone in 4× and 8× conditions, respectively. Indeed, the effect of Yoda1 on enhancing the poking-induced maximal whole-cell PIEZO1 currents and slowing down the inactivation tau has been previously reported (Wang et al., 2018) and was confirmed in this study. Interestingly, there was no difference in the median current elicited by M-Stim + Yoda1 in 1× conditions for mPIEZO1, probably due to Yoda1 causing more cells with lower channel expression, hence smaller current amplitudes, to cross the detection threshold of −100 pA, thereby lowering the median. Taken together, these data confirm that our M-Stim approach does not trigger saturating PIEZO1 currents, in contrast to other M-Stim techniques available in the literature (Coste et al., 2010; Syeda et al., 2016; Li et al., 2014; Ranade et al., 2014; Poole et al., 2014). Moreover, even in the presence of Yoda1, it remains unclear whether the current would saturate given the poor Yoda1 solubility at concentrations higher than 30 µM (Syeda et al., 2015) as well as the impossibility of testing pipetting flows above 110 µl/s with our approach/device, which currently represents a limitation of our technique.

To the best of our knowledge, we present a method that generates a potentially physiologically relevant mechanical stimulus, when considering e.g., the shear stress of the blood flow acting on the PIEZO1 channels expressed in the endothelial cells (Li et al., 2014), and provide for the first time an approach that combines high-throughput recordings (up to 384 cells/wells in parallel) and a direct read-out of PIEZO1 channels activity. In fact, the patch clamp studies on mechanical activation of PIEZO1 channels to date are based on selected single-cell recordings that focused on the careful characterization of PIEZO1 and typically do not specify a success rate. Here, we specifically aimed at establishing a highly parallelized, objectified approach to allow for the recording of mechanically induced PIEZO1 activation, enabling characterization of the channel as well as studying mutants and screening compounds, with the ultimate goal of accelerating the development of new medical strategies.

Data availability
The data underlying Figs. 1, 2, 3, S1, S2, and S3 are available in the published article itself, as well as in the supplementary tables where we provide statistical analyses of all data sets. The data are available from the corresponding author upon reasonable request.

References
Bae, C., R. Gnanasambandam, C. Nicolai, F. Sachs, and P.A. Gottlieb. 2013a. Xerocytosis is caused by mutations that alter the kinetics of the mechanosensitive channel PIEZO1. Proc. Natl. Acad. Sci. USA. 110:E1162–E1168. https://doi.org/10.1073/pnas.1219777110

Bae, C., P.A. Gottlieb, and F. Sachs. 2013b. Human PIEZO1: Removing inactivation. Biophys. J. 105:880–886. https://doi.org/10.1016/j.bpj.2013.07.019

Beech, D.J., and A.C. Kalli. 2019. Force sensing by piezo channels in cardiovascular health and disease. Arterioscler. Thromb. Vasc. Biol. 39:2228–2239. https://doi.org/10.1161/ATVBAHA.119.313348

Blythe, N.M., K. Muraki, M.J. Ludlow, V. Stylianidis, H.T.J. Gilbert, E.L. Evans, K. Cuthbertson, R. Foster, J. Swift, J. Li, et al. 2019. Mechanically activated Piezo1 channels of cardiac fibroblasts stimulate p38 mitogen-activated protein kinase activity and interleukin-6 secretion. J. Biol. Chem. 294:17395–17408. https://doi.org/10.1074/jbc.RA119.009167

Botello-Smith, W.M., W. Jiang, H. Zhang, A.D. Ozkan, Y.-C. Lin, C.N. Pham, J.J. Lacroix, and Y. Luo. 2019. A mechanism for the activation of the mechanosensitive Piezo1 channel by the small molecule Yoda1. Nat. Commun. 10:4503. https://doi.org/10.1038/s41467-019-12501-1

Coste, B., J. Mathur, M. Schmidt, T.J. Earley, S. Ranade, M.J. Petrus, A.E. Dubin, and A. Patapoutian. 2010. Piezo1 and Piezo2 are essential

Murciano et al.
Mechanical activation of Piezo1 channels

Journal of General Physiology
https://doi.org/10.1085/jgp.202213132

10 of 11

components of distinct mechanically activated cation channels. *Science.* 330:55–60. https://doi.org/10.1126/science.1193270

Coste, B., B. Xiao, J.S. Santos, R. Syeda, J. Grandl, K.S. Spencer, S.E. Kim, M. Schmidt, J. Mathur, A.E. Dubin, et al. 2012. Piezo proteins are pore-forming subunits of mechanically activated channels. *Nature.* 483:176–181. https://doi.org/10.1038/nature10812

Douguet, D., and E. Honoré. 2019. Mammalian mechanoelectrical transduction: Structure and function of force-gated ion channels. *Cell.* 179:340–354. https://doi.org/10.1016/j.cell.2019.08.049

Dubin, A.E., S. Murthy, A.H. Lewis, L. Brosse, S.M. Cahalan, J. Grandl, B. Coste, and A. Patapoutian. 2017. Endogenous Piezo1 can confound mechanically activated channel identification and characterization. *Neuron.* 94:266–270.e3. https://doi.org/10.1016/j.neuron.2017.03.039

Evans, E.L., K. Cuthbertson, N. Endesh, B. Rode, N.M. Blythe, A.J. Hyman, S.J. Hall, H.J. Gaunt, M.J. Ludlow, R. Foster, and D.J. Beech. 2018. Yoda1 analogue (Dooku1) which antagonizes Yoda1-evoked activation of Piezo1 and aortic relaxation. *Br. J. Pharmacol.* 175:1744–1759. https://doi.org/10.1111/bph.14188

Evans, E.L., O.V. Povstyan, D. De Vecchis, F. Macrae, L. Lichtenstein, T.S. Futers, G. Parsonage, N.E. Humphreys, A. Adamson, A.C. Kalli, et al. 2020. RBCs prevent rapid PIEZO1 inactivation and expose slow deactivation as a mechanism of dehydrated hereditary stomatocytosis. *Blood.* 136:140–144. https://doi.org/10.1182/blood.2019004174

Fotiou, E., S. Martin-Almedina, M.A. Simpson, S. Lin, K. Gordon, G. Brice, G. Atton, I. Jeffery, D.C. Rees, C. Mignot, et al. 2015. Novel mutations in PIEZO1 cause an autosomal recessive generalized lymphatic dysplasia with non-immune hydrops fetalis. *Nat. Commun.* 6:8085. https://doi.org/10.1038/ncomms9085

Guo, Y.R., and R. MacKinnon. 2017. Structure-based membrane dome mechanism for Piezo mechanosensitivity. *Elife.* 6:e33660. https://doi.org/10.7554/eLife.33660

Karamatic Crew, V., L.A. Tilley, T.J. Satchwell, S.A. AlSubhi, B. Jones, F.A. Spring, P.J.Walser, C.Martins Freire, N.Murciano, M.G.Rotordam. et al. 2022. Missense mutations in PIEZO1, encoding the Piezo1 mechanosensor protein, define the Er red blood cell antigens. *Blood.* 141:135–146. https://doi.org/10.1182/blood.2022016504

Lacroix, J.J., W.M. Botello-Smith, and Y. Luo. 2018. Probing the gating mechanism of the mechanosensitive channel Piezo1 with the small molecule Yoda1. *Nat. Commun.* 9:2029. https://doi.org/10.1038/s41467-018-04405-3

Lewis, A.H., and J. Grandl. 2015. Mechanical sensitivity of Piezo1 ion channels can be tuned by cellular membrane tension. *Elife.* 4:e12088. https://doi.org/10.7554/eLife.12088

Li, J., B. Hou, S. Tumova, K. Muraki, A. Bruns, M.J. Ludlow, A. Sedo, A.J. Hyman, L. McKeown, R.S. Young, et al. 2014. Piezo1 integration of vascular architecture with physiological force. *Nature.* 515:279–282. https://doi.org/10.1038/nature13701

Lukacs, V., J. Mathur, R. Mao, P. Bayrak-Toydemir, M. Procter, S.M. Cahalan, H.J. Kim, M. Bandell, N. Longo, R.W. Day, et al. 2015. Impaired PIEZO1 function in patients with a novel autosomal recessive congenital lymphatic dysplasia. *Nat. Commun.* 6:8329. https://doi.org/10.1038/ncomms9329

Ma, S., S. Cahalan, G. LaMonte, N.D. Grubaugh, W. Zeng, S.E. Murthy, E. Paytas, R. Gamini, V. Lukacs, T. Whitwam, et al. 2018. Common PIEZO1 allele in african populations causes RBC dehydration and attenuates plasmodium infection. *Cell.* 173:443–455.e12. https://doi.org/10.1016/j.cell.2018.02.047

Maneshi, M.M., L. Ziegler, F. Sachs, S.Z. Hua, and P.A. Gottlieb. 2018. Enantiomeric Aβ peptides inhibit the fluid shear stress response of PIEZO1. *Sci. Rep.* 8:14267. https://doi.org/10.1038/s41598-018-32572-2

Del Mármol, J.I., K.K. Touhara, G. Croft, and R. MacKinnon. 2018. Piezo1 forms a slowly-inactivating mechanosensory channel in mouse embryonic stem cells. *Elife.* 7:e33149. https://doi.org/10.7554/eLife.33149

Moroni, M., M.R. Servin-Vences, R. Fleischer, O. Sánchez-Carranza, and G.R. Lewin. 2018. Voltage gating of mechanosensitive PIEZO channels. *Nat. Commun.* 9:1096. https://doi.org/10.1038/s41467-018-03502-y

Murthy, S.E., A.E. Dubin, and A. Patapoutian. 2017. Piezos thrive under pressure: Mechanically activated ion channels in health and disease. *Nat. Rev. Mol. Cell Biol.* 18:771–783. https://doi.org/10.1038/nrm.2017.92

Nourse, J.L., and M.M. Pathak. 2017. How cells channel their stress: Interplay between Piezo1 and the cytoskeleton. *Semin. Cell Dev. Biol.* 71:3–12. https://doi.org/10.1016/j.semcdb.2017.06.018

Obergrussberger, A., S. Friis, A. Brüggemann, and N. Fertig. 2021. Automated patch clamp in drug discovery: Major breakthroughs and innovation in the last decade. *Expert Opin. Drug Discov.* 16:1–5. https://doi.org/10.1080/17460441.2020.1791079

Obergrussberger, A., T.A. Goetze, N. Brinkwirth, N. Becker, S. Friis, M. Rapedius, C. Haarmann, I. Rinke-Weiß, S. Stölzle-Feix, A. Brüggemann, et al. 2018. An update on the advancing high-throughput screening techniques for patch clamp-based ion channel screens: Implications for drug discovery. *Expert Opin. Drug Discov.* 13:269–277. https://doi.org/10.1080/17460441.2018.1428555

Obergrussberger, A., I. Rinke-Weiß, T.A. Goetze, M. Rapedius, N. Brinkwirth, N. Becker, M.G. Rotordam, L. Hutchison, P. Madau, D. Pau, et al. 2022. The suitability of high throughput automated patch clamp for physiological applications. *J. Physiol.* 600:277–297. https://doi.org/10.1113/JP282107

Parsonage, G., K. Cuthbertson, N. Endesh, N. Murciano, A.J. Hyman, C.H.Revill, O.V.Povstyan, E.Chunthapursat-Bon, M.Debant, M.J.Ludlow, et al. 2023. Improved PIEZO1 agonism through 4-benzoic acid modification of Yoda1. *Br. J. Pharmacol.* 180:2039–2063. https://doi.org/10.1111/bph.15996

Peralta, F.A., M. Balcon, A. Martz, D. Biljali, F. Cevoli, B. Arnould, A. Taly, T. Chataigneau, and T. Grutter. 2023. Optical control of PIEZO1 channels. *Nat. Commun.* 14:1269. https://doi.org/10.1038/s41467-023-36931-0

Peyronnet, R., J.R. Martins, F. Duprat, S. Demolombe, M. Arhatte, M. Jodar, M. Tauc, C. Duranton, M. Paulais, J. Teulon, et al. 2013. Piezo1-dependent stretch-activated channels are inhibited by Polycystin-2 in renal tubular epithelial cells. *EMBO Rep.* 14:1143–1148. https://doi.org/10.1038/embor.2013.170

Poole, K., R. Herget, L. Lapatsina, H.-D. Ngo, and G.R. Lewin. 2014. Tuning Piezo ion channels to detect molecular-scale movements relevant for fine touch. *Nat. Commun.* 5:3520. https://doi.org/10.1038/ncomms4520

Ranade, S.S., Z. Qiu, S.-H. Woo, S.S. Hur, S.E. Murthy, S.M. Cahalan, J. Xu, J. Mathur, M. Bandell, B. Coste, et al. 2014. Piezo1, a mechanically activated ion channel, is required for vascular development in mice. *Proc. Natl. Acad. Sci. USA.* 111:10347–10352. https://doi.org/10.1073/pnas.1409233111

Rode, B., J. Shi, N. Endesh, M.J. Drinkhill, P.J. Webster, S.J. Lotteau, M.A. Bailey, N.Y. Yuldasheva, M.J. Ludlow, R.M. Cubbon, et al. 2017. Piezo1 channels sense whole body physical activity to reset cardiovascular homeostasis and enhance performance. *Nat. Commun.* 8:350. https://doi.org/10.1038/s41467-017-00429-3

Rotordam, M.G., E. Fermo, N. Becker, W. Barcellini, A. Brüggemann, N. Fertig, S. Egée, M. Rapedius, P. Bianchi, and L. Kaestner. 2019. A novel gain-of-function mutation of Piezo1 is functionally affirmed in red blood cells by high-throughput patch clamp. *Haematologica.* 104:e179–e183. https://doi.org/10.3324/haematol.2018.201160

Shi, J., A.J. Hyman, D. De Vecchis, J. Chong, L. Lichtenstein, T.S. Futers, M. Rouahi, A.N. Salvayre, N. Auge, A.C. Kalli, and D.J. Beech. 2020. Sphingomyelinase disables inactivation in endogenous PIEZO1 channels. *Cell Rep.* 33:108225. https://doi.org/10.1016/j.celrep.2020.108225

Syeda, R., M.N. Florendo, C.D. Cox, J.M. Kefauver, J.S. Santos, B. Martinac, and A. Patapoutian. 2016. Piezo1 channels are inherently mechanosensitive. *Cell Rep.* 17:1739–1746. https://doi.org/10.1016/j.celrep.2016.10.033

Syeda, R., J. Xu, A.E. Dubin, B. Coste, J. Mathur, T. Huynh, J. Matzen, J. Lao, D.C. Tully, I.H. Engels, et al. 2015. Chemical activation of the mechanotransduction channel Piezo1. *Elife.* 4:e07369. https://doi.org/10.7554/eLife.07369

Tu, C.V., and D.H. Wood. 1996. Wall pressure and shear stress measurements beneath an impinging jet. *Exp. Therm. Fluid Sci.* 13:364–373. https://doi.org/10.1016/S0894-1777(96)00093-3

Wang, L., H. Zhou, M. Zhang, W. Liu, T. Deng, Q. Zhao, Y. Li, J. Lei, X. Li, and B. Xiao. 2019. Structure and mechanogating of the mammalian tactile channel PIEZO2. *Nature.* 573:225–229. https://doi.org/10.1038/s41586-019-1505-8

Wang, Y., S. Chi, H. Guo, G. Li, L. Wang, Q. Zhao, Y. Rao, L. Zu, W. He, and B. Xiao. 2018. A lever-like transduction pathway for long-distance chemical- and mechano-gating of the mechanosensitive Piezo1 channel. *Nat. Commun.* 9:1300. https://doi.org/10.1038/s41467-018-03570-9

Wijerathne, T.D., A.D. Ozkan, and J.J. Lacroix. 2022. Yoda1's energetic footprint on Piezo1 channels and its modulation by voltage and temperature. *Proc. Natl. Acad. Sci. USA.* 119:e2202269119. https://doi.org/10.1073/pnas.2202269119

Wu, J., A.H. Lewis, and J. Grandl. 2017. Touch, tension, and transduction—the function and regulation of piezo ion channels. *Trends Biochem. Sci.* 42:57–71. https://doi.org/10.1016/j.tibs.2016.09.004

Wyatt, T., B. Baum, and G. Charras. 2016. A question of time: Tissue adaptation to mechanical forces. *Curr. Opin. Cell Biol.* 38:68–73. https://doi.org/10.1016/j.ceb.2016.02.012

Zarychanski, R., V.P. Schulz, B.L. Houston, Y. Maksimova, D.S. Houston, B. Smith, J. Rinehart, and P.G. Gallagher. 2012. Mutations in the mechanotransduction protein PIEZO1 are associated with hereditary xerocytosis. *Blood.* 120:1908–1915. https://doi.org/10.1182/blood-2012-04-422253
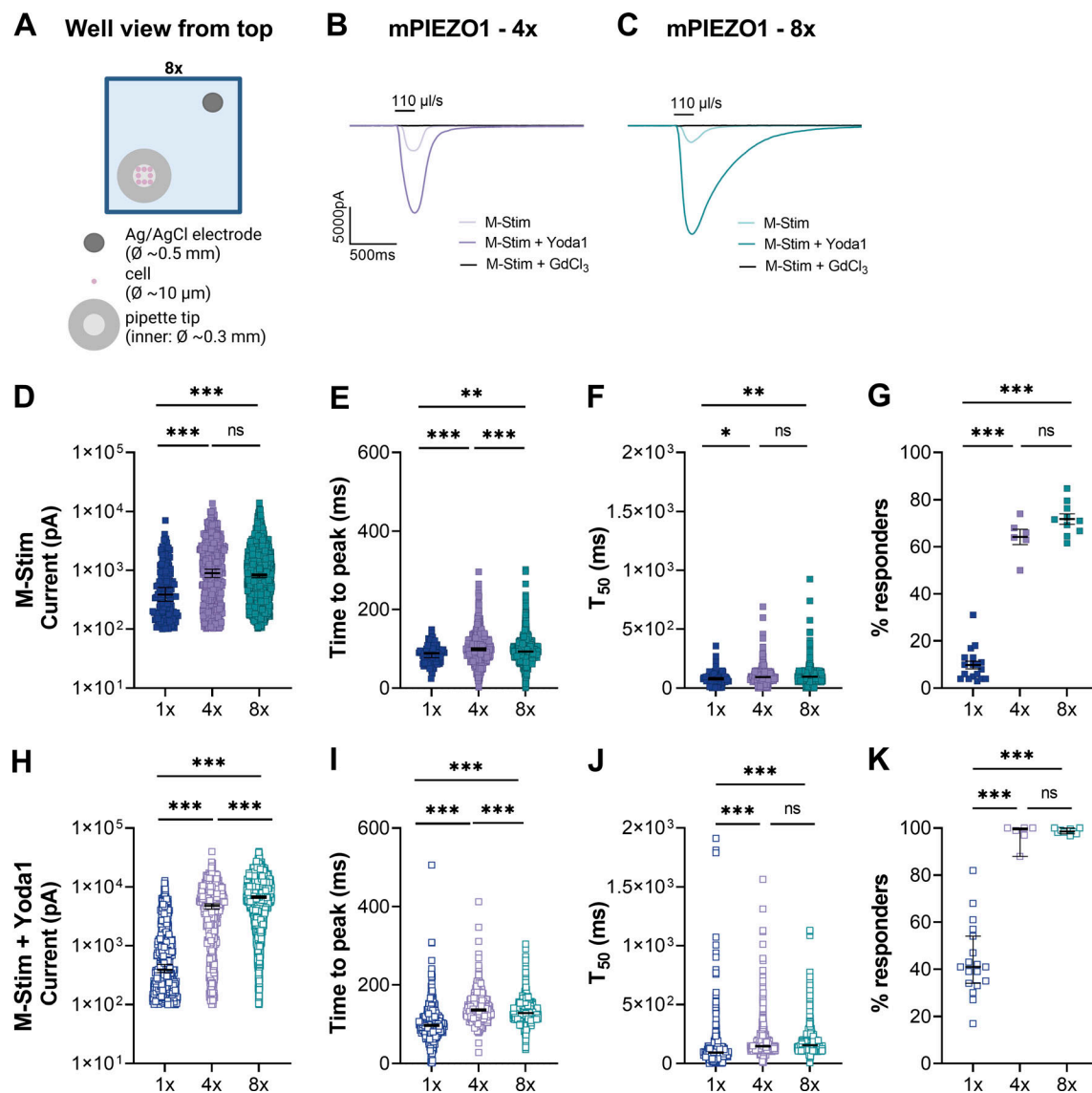
Figure S1. M-Stim approach using 8× chips. (A) Schematic illustration of the top view of one well of an NPC-384 chip with eight patch holes created with BioRender.com. **(B and C)** Representative mPIEZO1 inward current raw traces recorded from a 4× chip (B) and 8× chip (C) elicited by M-Stim and M-Stim + Yoda1. **(D and H)** Absolute current values of mPIEZO1 elicited by M-Stim (D) and M-Stim + Yoda1 (H) recorded from single-hole chips (1×, dark blue), four-hole chips (4×, purple), and eight-hole chips (8×, green), (M-Stim: 1×, $n = 148/1,910$; $N = 18$; 4×, $n = 579/941$; $N = 6$; 8×, $n = 1,845/2,831$; $N = 10$; ****$P < 0.0001$; M-Stim + Yoda1: 1×, $n = 693/1,785$; $N = 18$; 4×, $n = 685/722$; $N = 6$; 8×, $n = 2,425/2,459$; $N = 10$; ****$P < 0.0001$). **(E, F, I, and J)** Time to peak and T_{50} values (decay time from peak to 50% of the remaining signal) of mPIEZO1 elicited by M-Stim (E and F) and M-Stim + Yoda1 (I and J) recorded from 1× (dark blue), 4× chips (purple), and 8× (green) (M-Stim: 1×, $n = 88/1,440$; $N = 18$; 4×, $n = 506/941$; $N = 6$; 8×, $n = 1,528/2,831$; $N = 10$; ns $P > 0.05$, E: **$P = 0.009$, F: *$P = 0.02$, **$P = 0.001$, ****$P < 0.0001$; M-Stim + Yoda1: 1×, $n = 465/1,352$; $N = 18$; 4×, $n = 662/722$; $N = 6$; 8×, $n = 2,337/2,459$; $N = 10$; ns $P > 0.05$, ****$P < 0.0001$). **(G and K)** Percentage of mPIEZO1 wells responding to activation by M-Stim (G) and M-Stim + Yoda1 (K) at 110 µl/s pipetting flow using 1× chips (dark blue), 4× chips (purple), and 8× chips (green) (M-Stim: 1×, $N = 18$; 4×, $N = 6$; 8×, $N = 10$; M-Stim + Yoda1: 1×, $N = 18$; 4×, $N = 6$; 8×, $N = 10$; ns $P > 0.05$, ****$P < 0.0001$). Data are shown as values of individual cells with median and 95% CI (D–F and H–J), or as mean ± SEM (G and K), indicated in black, tested for statistical significance Mann-Whitney test, and unpaired t test. n represents the number of cells for a given experimental condition out of the total amount of valid cells, and N indicates the number of independent NPC-384 chips.
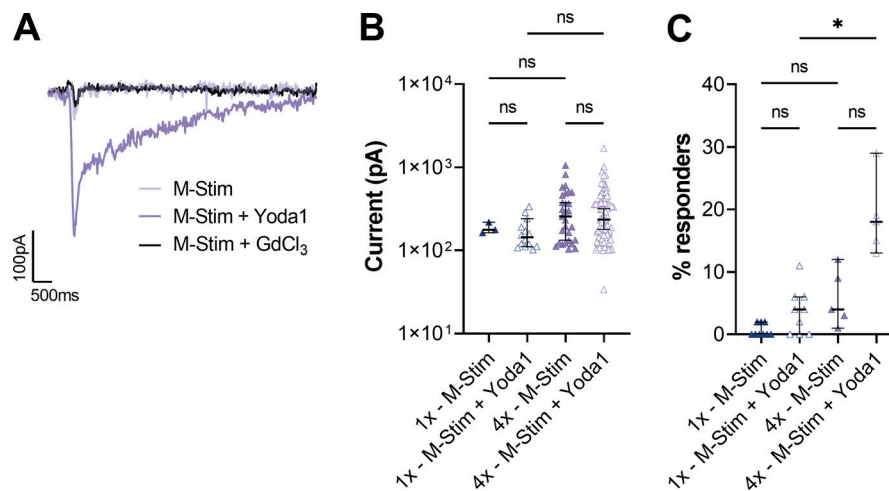
Figure S2. **Endogenous PIEZO1 activity in untransfected HEK293 cells recorded with 1× and 4× chips. (A)** Representative endogenous PIEZO1 inward current raw traces from one untransfected cell elicited by M-Stim (light purple trace) and M-Stim + Yoda1 (purple trace) and blocked by M-Stim + GdCl$_3$ (black trace) using a 4× chip. **(B)** Absolute current values of endogenous PIEZO1 from untransfected cells elicited by M-Stim and M-Stim + Yoda1 recorded from 1× chips (dark blue triangles) and 4× chips (purple triangles) (M-Stim: 1×, n = 3/432; N = 9; 4×, n = 29/485; N = 5; M-Stim + Yoda1: 1×, n = 14/449; N = 9; 4×, n = 82/448; N = 5 ns P > 0.05). **(C)** Percentage of wells from untransfected cells responding to activation by M-Stim and M-Stim + Yoda1 using 1× (dark blue triangles) and 4× chips (purple triangles) (M-Stim: 1×, N = 9; 4×, N = 5; M-Stim + Yoda1: 1×, N = 9; 4×, N = 5 ns P > 0.05, *P < 0.05). All data are shown as median and 95% CI, indicated in black, tested for statistical significance using Kruskal–Wallis test with Dunn's post-hoc test. n represents the number of cells for a given experimental condition out of total amount of valid cells, and N indicates the number of independent NPC-384 chips.
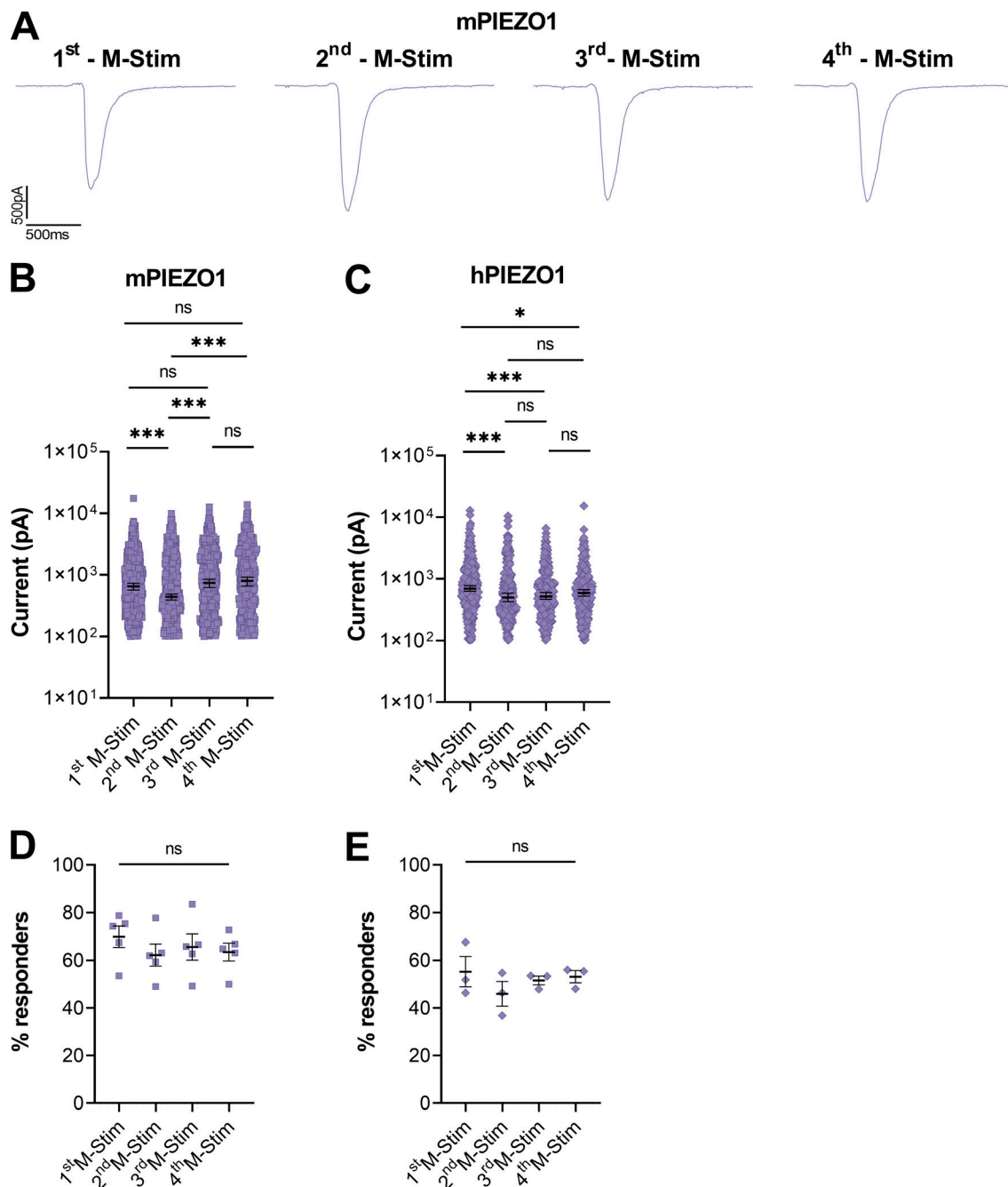
Figure S3. **Repeatability of the PIEZO1 signal over multiple M-Stim additions using 4× chips. (A)** Representative mPIEZO1 inward current raw traces of a single cell elicited by four M-Stim additions using 4× chip. **(B and C)** Absolute current values of mPIEZO1 (B) and hPIEZO (C) elicited by four M-Stim additions using 4× chips (mPIEZO1: first M-Stim, $n = 748/1,107$; second M-Stim $n = 594/1,002$; third M-Stim $n = 567/913$; fourth M-Stim $n = 510/838$; $N = 5$; ns $P > 0.05$, ****$P < 0.0001$; hPIEZO1: first M-Stim, $n = 388/752$; second M-Stim $n = 294/681$; third M-Stim $n = 317/626$; fourth M-Stim $n = 296/572$; $N = 3$, ns $P > 0.05$, *$P < 0.023$, ***$P < 0.0003$, ***$P < 0.0006$). **(D and E)** Percentage of mPIEZO1 (D) and hPIEZO1 (E) wells responding to activation by four identical M-Stim additions using 4× chips (mPIEZO1: $N = 5$; hPIEZO1: $N = 3$; ns $P > 0.05$). Data are shown as values of individual cells with median and 95% CI (B and C), or as mean ± SEM (D and E), indicated in black, tested for statistical significance using Kruskal-Wallis and ordinary one-way ANOVA with Dunn's and Tukey's post-hoc tests. n represents the number of cells for a given experimental condition out of the total amount of valid cells, and N indicates the number of independent NPC-384 chips.

Provided online are Table S1, Table S2, and Table S3. Table S1 shows the properties of mechanically activated signals elicited from mPIEZO1 and hPIEZO1 in various conditions. Table S2 shows endogenous PIEZO1 from untransfected cells. Table S3 shows mPIEZO1 and hPIEZO1 by four identical M-Stim applications.